RSC Advances

PAPER

View Article Online
View Journal | View Issue

Cite this: *RSC Adv.*, 2024, **14**, 29355

Restriction of reaction sites on metal-sulfide cores induced by steric repulsion of bis-N-heterocyclic carbene ligands in trinuclear complexes bearing triply bridging sulfide ligands†

Natsuki Yabune,[a] Hiroshi Nakajima [b] and Takanori Nishioka *[b]

Mixed-ligand and mixed-metal trinuclear complexes bearing two {Pt-bisNHC-C1} moieties, $[\{Pt(bisNHC\text{-}C1)\}_2(ML)(\mu_3\text{-}S)_2]^{n+}$ (ML = Pt(bisNHC-C2), $n = 2$; ML = Pt(bisNHC-C3), $n = 2$; ML = Rh(cod), $n = 1$; ML = RhCp*, $n = 2$), where bisNHC-C1, bisNHC-C2 and bisNHC-C3 represent methylene-, ethylene- and propylene-bridged bis-NHC ligands, respectively, were synthesised and structurally characterised. Reactions of these complexes with a half eq. of Ag(I) ions were examined using ^{1}H and ^{195}Pt NMR spectroscopy. The results exhibit that the trinuclear complexes react with Ag(I) ions accompanied by the formation of Ag–Pt bonds with the {Pt-bisNHC-C1} moieties in the first step affording corresponding heptanuclear complexes except for the RhCp* complex. The RhCp* complex gave a tetranuclear complex bearing the trinuclear unit with an Ag(I) ion. Further addition of Ag(I) ions for the other complexes resulted in disassembling of the heptanuclear clusters affording tetranuclear complexes confirmed by the observation of exchange of the Ag(I) ions in ^{195}Pt NMR measurements, which exhibited signals with no coupling to Ag nuclei.

Received 28th June 2024
Accepted 30th August 2024

DOI: 10.1039/d4ra01671h

rsc.li/rsc-advances

Introduction

In organic reactions catalysed by metal complexes, ancillary ligands of the complexes serve important roles for the selectivity of products in terms of steric effects. For the evaluation of steric bulkiness for phosphines and N-heterocyclic carbenes (NHCs) as ancillary ligands in their metal complexes, which have been used as catalysts for organic reactions, the cone angles[1] and the percent buried volume ($\%V_{bur}$)[2] are useful parameters. However, these symmetric evaluations are not suitable to explain the differences in steric effects in some cases because of the planar structures of NHC ligands affording unsymmetric steric repulsion. For example, change of a substituent for *i*-Pr to H, which derives only the 1% difference in $\%V_{bur}$, resulted in drastic improvement of the TONs 550 to 2200 for ethenolysis reactions of methyl oleate catalysed by mononuclear Ru complexes with monodentate NHC ligands.[3] Furthermore, in the case of bidentate chelating bis-NHC ligands, the dihedral angles between a coordination plane and each of the NHC planes in their square planar complexes change depending on the lengths of the alkylene linkers of the bis-NHC ligands (Fig. 1).[4] This feature of the bis-NHCs causes variation in steric hindrance around coordination sites of the metal centres of their complexes. Moreover, the bis-NHC ligands are rather flexible due to the alkylene linkers, and this character in structure affects steric repulsion around coordination sites. Especially for square planar complexes, in which the coordination sites on the coordination plane and the virtual axial

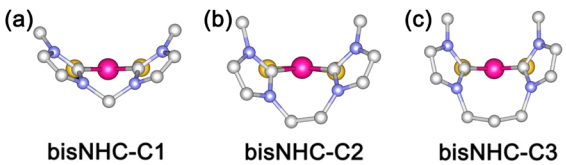

	bisNHC-C1	bisNHC-C2	bisNHC-C3
NHC–M	39.5(4)–46.5(3) [42(2)]	55.4(4)–64.0(3) [59(4)]	70.9(2)
NHC–NHC	107.0(6)–126.9(7) [110(3), 126.6(8)]	99.88(4)–103.0(5) [101.2(16)]	87.9(3)

Fig. 1 Ligand geometries of $\{PtC_2S_2\}$ units in (a) bisNHC-C1, (b) bisNHC-C2 and (c) bisNHC-C3 triplatinum complexes and table of dihedral angles (°, range [average]) between each NHC plane and coordination plane (NHC–M) and between NHC planes (NHC–NHC) obtained from crystallographic analyses of trinuclear complexes.

[a]*Division of Molecular Materials Science, Graduate School of Science, Osaka City University, Osaka 558-8585, Japan*

[b]*Department of Chemistry, Graduate School of Science, Osaka Metropolitan University, Osaka 558-8585, Japan. E-mail: nishioka@omu.ac.jp*

† Electronic supplementary information (ESI) available: Details of ^{195}Pt NMR spectroscopy, characterisation of new complexes (^{1}H and ^{13}C NMR spectra and ESI-mass spectra), DFT calculations and X-ray crystallography. CCDC 2238719–2238726. For ESI and crystallographic data in CIF or other electronic format see DOI: https://doi.org/10.1039/d4ra01671h

positions located vertically over the coordination plane are in different environments, arrangements of bis-NHC ligands form the coordination sphere with unsymmetric steric bulkiness.

We previously reported triplatinum complexes composed of three bis-NHC-Pt units bridged by two triply bridging sulfide ligands.[5] In the triplatinum complexes, each Pt ion has the square planar coordination geometry with two NHC carbon atoms and two sulfides (Fig. 2, red quadrilateral), and the neighbouring Pt ions connected by Pt–Pt bonds exist near the virtual axial positions (Fig. 2, blue). These triplatinum complexes react with Ag(I) ions to afford two kinds of heptanuclear clusters. Both heptanuclear clusters consist of two triplatinum moieties, which involve two sulfides and three bis-NHC ligands, and one Ag(I) ion as a bridging part. One of the heptanuclear clusters involves four Ag–Pt bonds (Fig. 3(a))[6] and the other possesses two Ag–S bonds (Fig. 3(b)).[7] The difference of the products is attributed to the steric bulkiness of the bis-NHC ligands. The methylene-bridged bis-NHC ligands with methyl substituents (bisNHC-C1), which have large dihedral angle between two NHC planes and then nearly planar structure, prevent the approach of Ag(I) ions to the sulfide ligands by the steric repulsion of the methyl substituents. In this situation, one of the Pt–Pt bonds locates in the less hindered space resulting in the formation of the Ag–Pt bonds. On the other hand, the ethylene-bridged bis-NHC ligands (bisNHC-C2) have the bent structure and cover the Pt–Pt bonds in the triplatinum complex to inhibit the Ag–Pt bond formation. In this case, the sulfide ligands are rather exposed due to the tilted methyl groups in the bis-NHC ligands resulting in the formation of the Ag–S bonds. These clearly appeared steric effects are the results of the enhanced steric repulsion by the crowded environment of the ancillary bis-NHC ligands in the trinuclear system.

These results suggest that the bis-NHC trinuclear system is one of the best candidates for investigation of the steric repulsion of bis-NHC ligands in square planar complexes, which are often used as catalysts. In this study, we focus on the reactions of Ag(I) ions and trinuclear complexes bearing the diplatinum unit with the bisNHC-C1 ligands, which could be an essential component for the formation of the Ag–Pt bonds, and another metal–ligand moiety such as platinum with the bisNHC-C2 or propylene-bridged bis-NHC (bisNHC-C3) ligands and rhodium with 1,5-cyclooctadiene (cod) or 1,2,3,4,5-pentamethyl cyclopentadienyl (Cp*) ligands. The bisNHC-C1 ligands in the diplatinum moiety of the trinuclear complexes can move away from each other for the formation of the Ag–Pt bonds. The incorporated other metal–ligand units into the trinuclear

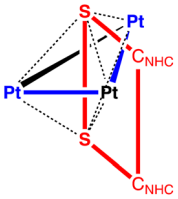

Fig. 2 Coordination plane of one of three Pt(II) ions in trinuclear complex bearing sulfide and NHC ligands.

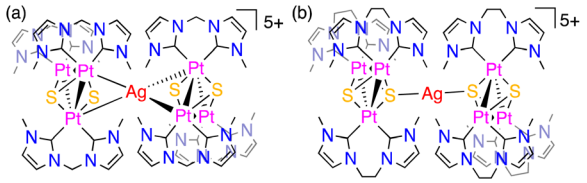

Fig. 3 Heptanuclear complexes (a) with Ag–Pt and (b) with Ag–S bonds.

complexes would work to tune the steric effects of the bisNHC-C1 ligands on the reactions with Ag(I) ions *via* steric repulsion of the ancillary ligands in the other metal–ligand units with the bisNHC-C1 ligands. In this study, we describe the unsymmetric steric effects of bis-NHC ligands for square planar complexes, which appeared for the reaction sites of the trinuclear complexes in the reactions with Ag(I) ions.

Results and discussion

Syntheses of mixed-ligand and mixed-metal trinuclear complexes

Mixed-ligand triplatinum complexes, $[\{Pt(bisNHC\text{-}C1)\}_2\{Pt(bisNHC\text{-}Cn)\}(\mu_3\text{-}S)_2]^{2+}$ ($n = 2$, $[\mathbf{Pt^{C1}_2Pt^{C2}}]^{2+}$; $n = 3$, $[\mathbf{Pt^{C1}_2Pt^{C3}}]^{2+}$), were synthesised by the one-pot reactions of *cis*-[Pt(bisNHC-C2)$(SH)_2$] or *cis*-[Pt(bisNHC-C3)$(SH)_2$] and 2 eq. of *cis*-[Pt(bisNHC-C1)Cl_2] in the presence of $KHCO_3$ as a proton scavenger (Scheme 1(a)). On the other hand, mixed-metal trinuclear complexes, $[\{Pt(bisNHC\text{-}C1)\}_2(ML)(\mu_3\text{-}S)_2]^{n+}$ (ML = Rh(cod), $n = 1$, $[\mathbf{Pt^{C1}_2Rh^{cod}}]^{+}$; ML = RhCp*, $n = 2$, $[\mathbf{Pt^{C1}_2Rh^{Cp^*}}]^{2+}$), were synthesised by two-step reactions (Scheme 1(b) and (c)). In the first step for the synthesis of $[\mathbf{Pt^{C1}_2Rh^{cod}}]^{+}$, a bis-sulfide-bridged dinuclear platinum complex with the bisNHC-C1 ligands was generated by the reaction of mononuclear complexes, *cis*-[Pt(bisNHC-C1)$(SH)_2$] and *cis*-[Pt(bisNHC-C1)Cl_2]. The addition of 0.5 eq. of $[\{Rh(cod)\}_2(\mu\text{-}Cl)_2]$ to the solution in the second step afforded $[\mathbf{Pt^{C1}_2Rh^{cod}}]^{+}$. In the case of

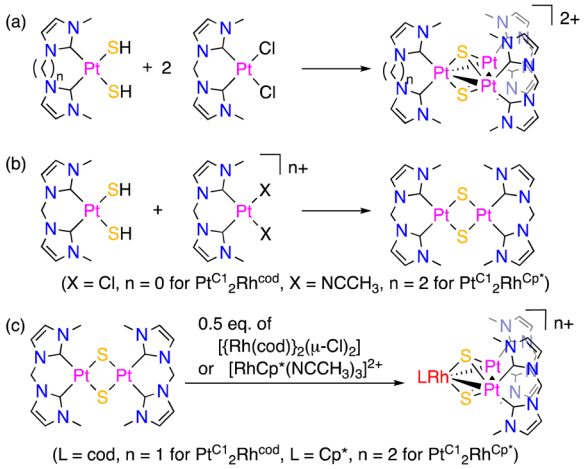

Scheme 1 (a) One pot reaction for mixed-ligand triplatinum complexes and (b) the first and (c) second reactions of two-step syntheses for mixed-metal trinuclear complexes.

$[Pt^{C1}{}_2Rh^{Cp*}]^{2+}$, the bis-(acetonitrile)platinum complex, *cis*-$[Pt(bisNHC\text{-}C1)(NCCH_3)_2]^{2+}$, was used instead of the dichloro complex to obtain the bis-sulfide-bridged dinuclear complex in the first step. In the second step, $[RhCp^*(NCCH_3)_3]^{2+}$ was added to give $[Pt^{C1}{}_2Rh^{Cp*}]^{2+}$. Removal of the chloride ions from the reaction system improved the yield of $[Pt^{C1}{}_2Rh^{Cp*}]^{2+}$ probably because the unfavourable interaction between the Rh(III) centre and chloride ions, which disturbs the reaction with sulfide ligands, could be avoided. Syntheses of mixed metal–ligand trinuclear complexes with two triply bridging sulfide ligands using the reactions of a bis-sulfide-bridged diplatinum complex and an additional metal–ligand unit were reported for diplatinum phosphine and arsine complexes.[8]

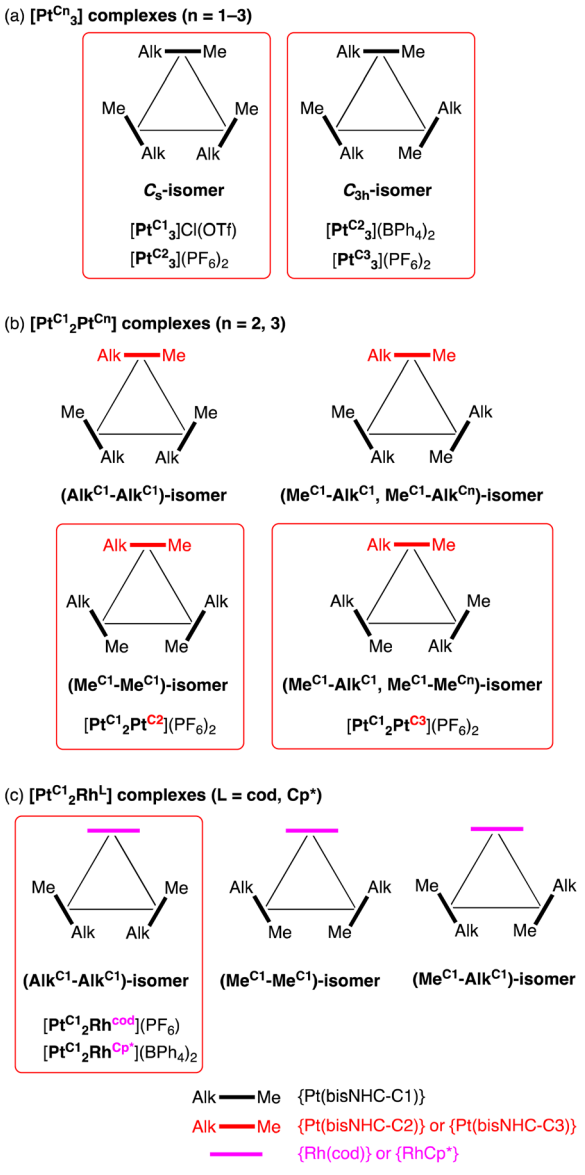

Fig. 4 Possible isomers for (a) triplatinum, (b) mixed-ligand triplatinum and (c) mixed-metal trinuclear complexes bearing bis-NHC ligands. "Me" and "Alk" show relative positions of the methyl substituents and alkylene bridges of bisN-HC ligands, respectively. Red squares represent observed isomers in X-ray crystallography.

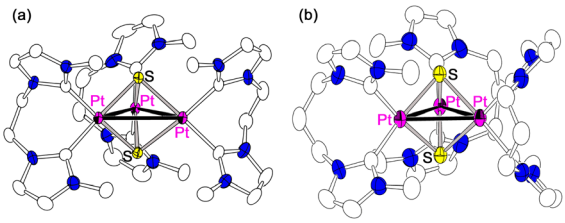

Fig. 5 Structures of triplatinum complexes with (a) bisNHC-C2 and (b) bisNHC-C3 ligands.

Structures of trinuclear complexes in the solid state

The structures of $[Pt^{C1}{}_3]Cl(OTf)$[6] and $[Pt^{C2}{}_3](BPh_4)_2$[5] were previously analysed by X-ray crystallography. In this study, X-ray crystallographic analyses for $[Pt^{C2}{}_3](PF_6)_2$, $[Pt^{C3}{}_3](PF_6)_2$, $[Pt^{C1}{}_2Pt^{C2}](PF_6)_2$, $[Pt^{C1}{}_2Pt^{C3}](PF_6)_2$, $[Pt^{C1}{}_2Rh^{cod}](PF_6)$ and $[Pt^{C1}{}_2Rh^{Cp*}](BPh_4)_2$ were performed showing that crystals containing one of the isomers of each complex were obtained, although there are some possible isomers attributed to the orientation of the bis-NHC ligands (Fig. 4). The crystallographic analysis of the PF_6 salt of $[Pt^{C2}{}_3]^{2+}$ indicates that the complex cation adopts the C_s-isomeric form (Fig. 5(a)), whereas the previously reported analysis for the BPh_4 salt exhibited that the crystal contained only the C_{3h}-isomer.[5] On the other hand, $[Pt^{C3}{}_3](PF_6)_2$ crystallised as the C_{3h}-isomer (Fig. 5(b)). These C_s- and C_{3h}-isomers are in equilibrium in solution,[5] and the crystal-packing with the counter anions leads the predominant crystallisation of each salt. Mixed-ligand triplatinum complexes, $[Pt^{C1}{}_2Pt^{C2}](PF_6)_2$ (Fig. 6(a)) and $[Pt^{C1}{}_2Pt^{C3}](PF_6)_2$ (Fig. 6(b)), crystallised as the (Me^{C1}-Me^{C1})- and (Me^{C1}-Alk^{C1}, Me^{C1}-Me^{C3})-isomers (Fig. 4(b)), respectively. Both of the crystallised Pt_2Rh mixed-metal complexes, $[Pt^{C1}{}_2Rh^{cod}](PF_6)$ (Fig. 7(a)) and $[Pt^{C1}{}_2Rh^{Cp*}](BPh_4)_2$ (Fig. 7(b)), are the (Alk^{C1}-Alk^{C1})-isomers (Fig. 4(c)).

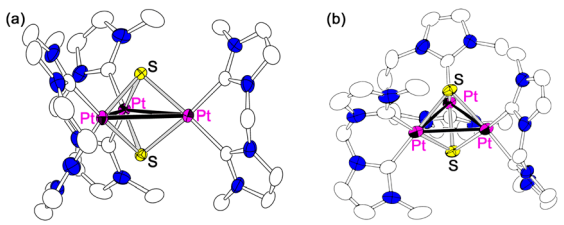

Fig. 6 Structures of mixed-ligand triplatinum complexes bearing two bisNHC-C1 and (a) bisNHC-C2 or (b) bisNHC-C3 ligands.

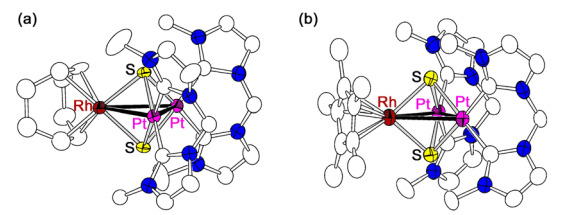

Fig. 7 Structures of mixed-metal trinuclear complexes bearing two {Pt-bisNHC-C1} units and (a) {Rh(cod)} or (b) {RhCp*} moieties. One of the positionally disordered cod or Cp* ligands is omitted for clarity (see ESI†).

Structures of trinuclear complexes in solution

Triplatinum complex with bisNHC-C3 ligands ($[Pt^{C3}{}_3]^{2+}$) in solution. Alkylene-bridged bis-NHC complexes exhibit dynamic behaviour in solution due to the flapping motion of the bis-NHC ligands.[5–7,9,10] Because of the dynamics, the isomers of each trinuclear complex shown in Fig. 4 are in equilibrium in solution, whereas one of the isomers for each complex is observed in the solid state. Similar to the previously reported bisNHC-C2 complex ($[Pt^{C2}{}_3]^{2+}$),[5] the $[Pt^{C3}{}_3]^{2+}$ complex showed four sets of signals for the bisNHC-C3 ligands assignable to the C_s- and C_{3h}-isomers, which exhibit three sets and one set of ^{1}H NMR signals for the ligands, respectively (Fig. S1 in ESI†).

Mixed-ligand triplatinum complexes ($[Pt^{C1}{}_2Pt^{C2}]^{2+}$ and $[Pt^{C1}{}_2Pt^{C3}]^{2+}$) in solution. For the mixed-ligand triplatinum complex with the bisNHC-C1 and bisNHC-C2 ligands, $[Pt^{C1}{}_2Pt^{C2}]^{2+}$, ^{1}H NMR spectra showed broad signals at 293 K due to the equilibrium of the isomers (Fig. S2(a) in ESI†), and several sets of sharp signals for the bis-NHC ligands at 253 K (Fig. S2(b)†). There are four possible isomers for $[Pt^{C1}{}_2Pt^{C2}]^{2+}$ as shown in Fig. 4(b), and each isomer bearing two inequivalent bisNHC-C1 and one bisNHC-C2 ligands should exhibit three sets of ^{1}H NMR signals for the ligands. In this point of view, the ^{1}H NMR measurements showed that multiple isomers of $[Pt^{C1}{}_2Pt^{C2}]^{2+}$ exist in solution and they are in equilibrium. Existence of the multiple isomers in solution is also supported by the ^{195}Pt NMR measurement showing at least three sets of three signals in the range of −4000 to −3500 ppm (Fig. S14 bottom in ESI†).

On the other hand, $[Pt^{C1}{}_2Pt^{C3}]^{2+}$ exhibits different behaviour in ^{1}H NMR measurements. For $[Pt^{C1}{}_2Pt^{C3}]^{2+}$, only the signals for two bisNHC-C1 and one bisNHC-C3 ligands were observed in the ^{1}H NMR spectra at both 293 K (Fig. S3(a) in ESI) and 253 K (Fig. S3(b)†). While $[Pt^{C1}{}_2Pt^{C3}]^{2+}$ complex can also adopt four isomeric structures similar to $[Pt^{C1}{}_2Pt^{C2}]^{2+}$, the results indicate that the equilibrium shifts drastically to one of the four isomers in solution. The broadening of the signals at higher temperature suggests that the interconversion between the isomers is slower than the NMR time scale. This result is consistent with the observation of one set of three signals with satellite peaks at −3637 ($^1J_{Pt-Pt}$ = 735 Hz), −3697 ($^1J_{Pt-Pt}$ = 723 Hz) and −3791 ppm ($^1J_{Pt-Pt}$ = 771 Hz) in the ^{195}Pt NMR spectrum (Fig. S15 bottom in ESI†). The observation of only one of the isomers existing in solution probably ascribes to the larger steric repulsion of the bisNHC-C3 ligands along the Pt_3 plane in the triplatinum complex than the bisNHC-C2 in the corresponding trinuclear complex. To avoid the large steric repulsion with the methyl groups or the propylene bridge of the bisNHC-3 ligands, the methyl groups in one of the bisNHC-C1 ligands face to the methyl groups of the bisNHC-C3 ligand with the offset orientations. This offset orientation of the methyl groups between the bisNHC-C1 and bisNHC-C3 ligands and the smaller steric repulsion between the methyl groups and the methylene bridge of the bisNHC-C1 ligands result in the stabilisation of the (Me^{C1}-Alk^{C1}, Me^{C1}-Me^{C3})-isomeric form of the complex, which is observed in the crystallographic analysis.

Mixed-metal diplatinum–rhodium complexes ($[Pt^{C1}{}_2Rh^{cod}]^+$ and $[Pt^{C1}{}_2Rh^{Cp^*}]^{2+}$) in solution. Each of the mixed-metal Pt_2Rh trinuclear complexes, $[Pt^{C1}{}_2Rh^{cod}]^+$ and $[Pt^{C1}{}_2Rh^{Cp^*}]^{2+}$, shows a set of relatively broad signals in the ^{1}H NMR spectrum at 293 K for the bisNHC-C1 and cod or Cp* ligands (Fig. S4(a) and S5(a) in ESI†). These signals observed in each ^{1}H NMR spectrum at 293 K are assignable to one of the isomers of each complex and they appeared as sharp signals at 253 K (Fig. S4(b) and S5(b)†). These results indicate that the isomers shown in Fig. 4(c) are in equilibrium and the equilibrium extremely shifts to one of the isomers similar to the $[Pt^{C1}{}_2Pt^{C3}]^{2+}$ mixed-ligand complex. The ^{195}Pt NMR measurements affording one singlet signal at −3887 or −4007 ppm for each of the mixed-metal trinuclear complexes, $[Pt^{C1}{}_2Rh^{cod}]^+$ and $[Pt^{C1}{}_2Rh^{Cp^*}]^{2+}$, respectively, also revealed that the two Pt centres in each complex are equivalent (Fig. S16 and S17 bottoms in ESI†). The predominant isomers of the mixed-metal Pt_2Rh complexes in solution are probably the ones observed in the crystallographic analyses and have the two equivalent bisNHC-C1 ligands facing to each other *via* the methylene bridges.

Elucidation of steric effects of ligands in trinuclear complexes on their reactions with Ag(I) salt

As previously reported, the reactions of the triplatinum complexes bearing the bisNHC-C1 or bisNHC-C2 ligands with Ag(I) ions yielded the Pt_3AgPt_3 heptanuclear complexes, in which each Ag(I) ion bridges two triplatinum units *via* four Ag–Pt[6] or two Ag–S bonds,[7] respectively. The formation of the different products is attributed to the steric repulsion along the Pt_3 plane or around the sulfide ligands depending on the geometry of the bis-NHC ligands, which are determined by the lengths of the alkylene bridges. The bisNHC-C1 ligands coordinating to the platinum centres allow the Ag(I) ions to approach the platinum centres and prevent the coordination of the sulfide ligands, while the bisNHC-C2 ligands act the opposite roles. Here, the steric effects of the bis-NHC ligands were elucidated using reactions of trinuclear complexes bearing two {Pt(bisNHC-C1)} moieties, which could be essential part for the Ag–Pt bond formation, and another metal–ligand unit with Ag(I) ions. In addition, to assess the steric effects of the bisNHC-C3 ligand, reaction with Ag(I) ions was also examined for a triplatinum complex with three bisNHC-C3 ligands. The ligands bring larger steric repulsion along the Pt_3 plane and afford more space around the sulfide ligands due to its rather folded structure derived from the nearly vertical dihedral angle between each NHC moiety and the coordination plane. The reactions were monitored by ^{1}H and ^{195}Pt NMR spectroscopy using a mixture of each trinuclear complex with an appropriate amount of silver salt to give Ag-adducts of the trinuclear complexes. The chemical shifts and coupling constants of the ^{195}Pt NMR signals for the trinuclear complexes and their reaction mixtures with Ag(I) ions are listed in Table 1. Here, the reactions of the trinuclear complexes with 0.5 eq. of Ag(I) salt are described first to exhibit the initial step of the reactions. In the second, the rather complicated equilibrium involving the trinuclear complexes with more Ag(I) salt showing the other

Table 1 ^{195}Pt NMR signals (chemical shift in ppm ($^{1}J_{Pt-X}$/Hz, X)) for trinuclear complexes and their reaction mixtures with Ag(I) ions (Fig. S11–S17)

	$[Pt^{C1}_3]^{2+}$	$[Pt^{C2}_3]^{2+}$	$[Pt^{C3}_3]^{2+}$	$[Pt^{C1}_2Pt^{C2}]^{2+}$	$[Pt^{C1}_2Pt^{C3}]^{2+}$	$[Pt^{C1}_2Rh^{cod}]^{+}$	$[Pt^{C1}_2Rh^{Cp*}]^{2+}$
Complex	**−3608 (779, Pt)** **−3644 (1020, Pt)** −3729* **−3891 (1052, Pt; 771, Pt)**	−3471 −3517 **−3612*** −3738	**−3641***	−3552 −3784 **−3582 −3788** −3593 −3865 −3621 −3956 **−3626**	**−3637 (735, Pt)** **−3697 (723, Pt)** **−3791 (771, Pt)**	**−3887**	**−4007**
+ 0.5 eq. Ag^+	**−3155 (554, Ag)** **−3446 (526, Ag)** **−3828 (2020, Pt; 1008, Pt)**	**−3587**	−3566 (br) −3592 (br) **−3623** −3653 (br)	**−3168 (530, Ag)** **−3412 (538, Ag)** **−3739**	**−3263 (454, Ag)** **−3342 (518, Ag)** −3620 (br)** **−3827 (1743, Pt; 1444, Pt)**	**−3494 (432, Ag; 62, Rh)**	**−3554 (422, Ag; 68, Rh)**
+ ex. Ag^+	−3520 to −3515**	**−3569**	**−3600**	**−3420 to −3390(br)**	**−3359 (1197, Pt; 478, Pt)** **−3427 (1165, Pt; 426, Pt)** −3602 **−3848 (1205, Pt)** −3941 −4019	**−3533 (br)**	**−3589 (120, Rh)** −3603*** −3676***

Bold: predominant signals, red: Ag-bound Pt centre, blue: Ag-unbound Pt centre in complexes with Ag–Pt bonds. *C_{3h}-isomer. **Unknown products.

reaction sites on the metal sulfide cores in the complexes affected by the shapes of their ligands.

Reactions of trinuclear complexes with 0.5 eq. of Ag(I) salt

Reactions of triplatinum complexes with bisNHC-C1 ($[Pt^{C1}_3]^{2+}$) or bisNHC-C2 ligands ($[Pt^{C2}_3]^{2+}$) with 0.5 eq. of Ag(I) ions. Prior to discuss the reactions of the mixed-ligand and mixed-metal trinuclear complexes with Ag(I) ions, the results of ^{195}Pt NMR measurements for $[Pt^{C1}_3]^{2+}$, $[Pt^{C2}_3]^{2+}$ and the products in their reactions with 0.5 eq. of Ag(I) ions are presented. The obtained data about the coupling with Ag nuclei and the downfield shifts of signals in ^{195}Pt spectra of the known complexes and their Ag-adducts would help to evaluate the formation of Ag–Pt and Ag–S bonds in the reactions of the mixed-ligand and mixed-metal trinuclear complexes with Ag(I) ions.

^{195}Pt NMR spectrum of $[Pt^{C1}_3]^{2+}$ exhibited one singlet signal at −3729 ppm and three singlet signals with satellite peaks by the coupling with the neighbouring ^{195}Pt nuclei at −3891 ($^{1}J_{Pt-Pt}$ = 771 Hz, $^{1}J_{Pt-Pt}$ = 1052 Hz), −3644 ($^{1}J_{Pt-Pt}$ = 1020 Hz) and −3608 ($^{1}J_{Pt-Pt}$ = 779 Hz) ppm (Fig. S11 bottom in ESI†). While the symmetric C_{3h}-isomer, which has three equivalent Pt centres, showed no satellite peaks, the unsymmetric C_s-isomer, which involves three inequivalent Pt centres, exhibited the satellite peaks due to the coupling with the neighbouring ^{195}Pt nuclei. In the ^{195}Pt NMR spectrum of $[Pt^{C1}_3]^{2+}$ with 0.5 eq. of Ag(I) ions, two doublets at −3155 ($^{1}J_{Pt-Ag}$ = 554 Hz) and −3446 ppm ($^{1}J_{Pt-Ag}$ = 526 Hz) and one singlet with satellite peaks at −3828 ppm ($^{1}J_{Pt-Pt}$ = 2020 Hz, $^{1}J_{Pt-Pt}$ = 1008 Hz) were observed (Fig. S11 middle in ESI†). This observation is consistent with the formation of the Pt_3AgPt_3 heptanuclear complex with four Pt–Ag bonds, which involves the triplatinum units with the C_s-isomeric form bearing three inequivalent Pt centres (Scheme 2). The doublet signals are assigned to the Pt centres forming the Ag–Pt bonds and the singlet with satellite peaks is assignable to the Ag-unbound Pt centre. Additionally, satellite peaks for the doublet signals could not be detected due to the relatively diluted concentration of the sample to prevent the formation of precipitates of the product. Above mentioned results reveal that the formation of the Ag–Pt bonds causes the downfield shift by hundreds ppm and the splitting by the coupling with Ag nuclei for the ^{195}Pt NMR signals.

In the case of $[Pt^{C2}_3]^{2+}$, its ^{195}Pt NMR spectrum showed one intense singlet at −3612 ppm assignable to the C_{3h}-isomer and three weak singlets at −3738, −3517 and −3471 ppm for the C_S-isomers (Fig. S12 bottom in ESI†). Although the ^{195}Pt NMR signals for the C_s-isomer should appear with satellite peaks, no satellite signals could be detected in this concentration because

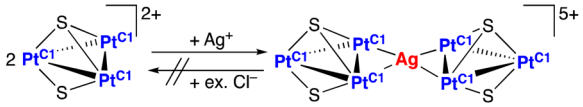

Scheme 2 Reactions of triplatinum complex with bisNHC-C1 ligands, $[Pt^{C1}_3]^{2+}$, with Ag(I) ions.

of the reduced intensities of the signals due to the three inequivalent Pt centres of the C_s-isomeric form and the equilibrium shifted to the C_{3h}-isomer. In the presence of 0.5 eq. of Ag(I) ions, $[\mathbf{Pt^{C2}}_3]^{2+}$ showed only one singlet signal at −3587 ppm in the ^{195}Pt NMR spectrum (Fig. S12 middle in ESI†). The downfield shift by dozens ppm is attributed to the formation of the Ag–S bonds.

Reaction of triplatinum complex with bisNHC-C3 ligands ($[\mathbf{Pt^{C3}}_3]^{2+}$) with 0.5 eq. of Ag(I) ions. While the ^{1}H NMR spectrum of $[\mathbf{Pt^{C3}}_3]^{2+}$ indicates that the C_{3h}- and C_s-isomers exist in equilibrium in solution (Fig. S6(a)†), the ^{195}Pt spectrum showed only one singlet signal at −3641 ppm assignable to the C_{3h}-isomer (Fig. S13 bottom in ESI†). The addition of 0.5 eq. of Ag(I) ions induced a shift of the ^{1}H NMR signals for the triplatinum complex unit with the C_{3h}-isomeric form (Fig. S6(b)†). On the other hand, no shift of the *N*-methyl signals for the complex with the C_s-isomeric form was observed. However, the intensities of the signals decreased by the addition of Ag(I) ions. Furthermore, addition of an appropriate amount of NH_4Cl led the formation of AgCl to eliminate Ag(I) ions from the reaction system and restored the signals for the triplatinum complex (Fig. S6(d)†). This recovery of the signals for the triplatinum complex indicates that the Ag(I) ions react with the sulfide ligands of the complex rather than the platinum centres (Scheme 3). The ^{195}Pt NMR spectrum of the triplatinum complex with 0.5 eq. of Ag(I) ions showed one large (−3623 ppm) and three small broad signals (−3566, −3592 and −3653 ppm) assignable to the C_{3h}- and C_s-isomeric forms, respectively (Fig. S13 middle in ESI†). These broad downfield shifted signals indicate the equilibrium between the C_s-isomer of the complex and the Ag-adduct with the C_{3h}-isomeric form bearing Ag–S bonds (Scheme 3). In the case of $[\mathbf{Pt^{C2}}_3]^{2+}$, the ^{1}H NMR signals for the C_s-isomer completely disappeared by the addition of Ag(I) ions as previously reported.[7] These differences are probably due to the space around the sulfide ligands. For the bisNHC-C3 complex, the dihedral angles between the coordination plane and each of the two NHC moieties are nearly vertical (Fig. 1) and then the *N*-methyl substituents are away from the sulfide ligands to provide more space for accessing of Ag(I) ions and solvent molecules. As a result, the coordinated Ag(I) ion could exchange with free Ag(I) ions more readily.

These results of ^{1}H and ^{195}Pt NMR spectroscopy and crystallography indicate that the bisNHC-C2 and bisNHC-C3 ligands prevent the Ag(I) ions approaching the platinum centres in their trinuclear complexes and some of the Ag-adducts with Ag–S bonds exist in equilibrium in solution.

Reactions of mixed-ligand triplatinum complexes with two bisNHC-C1 and one bisNHC-C2 ($[\mathbf{Pt^{C1}}_2\mathbf{Pt^{C2}}]^{2+}$) or bisNHC-C3 ($[\mathbf{Pt^{C1}}_2\mathbf{Pt^{C3}}]^{2+}$) with 0.5 eq. of Ag(I) ions. The triplatinum complex bearing three bisNHC-C1 ligands, $[\mathrm{Pt^{C1}}_3]^{2+}$, reacts with 0.5 eq. of Ag(I) ions to form the heptanuclear complex, in which two triplatinum units are bridged by an Ag(I) ion through four Ag–Pt bonds.[6] The Ag(I) ion in the heptanuclear complex is hardly extracted by the addition of chloride ions, and the heptanuclear structure remains intact in the presence of chloride ions in solution for at least a week at room temperature. The {[Pt(bisNHC-C1)]$_2$} diplatinum moiety provides the reaction sites for an Ag(I) ion to form the Ag–Pt bonds, and the ligands cover the Ag(I) ion in the heptanuclear complex to avoid the attack of solvent molecules such as acetonitrile. This diplatinum moiety seems to be required to form the Ag–Pt bonds with the triplatinum complexes. To examine the formation of such Ag–Pt bonds, reactions of the mixed-ligand triplatinum complexes with two bisNHC-C1 and one bisNHC-C2, $[\mathbf{Pt^{C1}}_2\mathbf{Pt^{C2}}]^{2+}$, or bisNHC-C3, $[\mathbf{Pt^{C1}}_2\mathbf{Pt^{C3}}]^{2+}$, with Ag(I) ions were monitored using ^{1}H and ^{195}Pt NMR spectroscopy.

Addition of 0.5 eq. of Ag(I) ions to a solution of mixed-ligand triplatinum complex $[\mathbf{Pt^{C1}}_2\mathbf{Pt^{C2}}]^{2+}$, which shows broad signals in the ^{1}H NMR spectrum (Fig. S7(a) in ESI†), afforded the observation of sharp signals (Fig. S7(b)†). This fact implies that the reaction of the complex with 0.5 eq. of Ag(I) ions affords the corresponding Pt_3AgPt_3 heptanuclear complex with the Ag–Pt bonds (Scheme 4). The ^{195}Pt NMR spectrum of the reaction mixture exhibited two doublets at −3168 ($^1J_{Pt-Ag}$ = 530 Hz) and −3412 ppm ($^1J_{Pt-Ag}$ = 538 Hz) and one singlet at −3739 ppm (Fig. S14 middle in ESI†). The observation of the downfield shift of the signals and the coupling with the Ag nucleus clearly shows the Ag–Pt bond formation with two of the three Pt centres.

The mixed-ligand complex with bisNHC-C3, $[\mathbf{Pt^{C1}}_2\mathbf{Pt^{C3}}]^{2+}$, exhibited similar spectral changes upon the addition of 0.5 eq. of Ag(I) ions (Fig. S8(b) in ESI†) to the bisNHC-C2 complex, $[\mathbf{Pt^{C1}}_2\mathbf{Pt^{C2}}]^{2+}$, indicating that the Ag-adduct with the Ag–Pt bonds forms at the first stage (Scheme 4). The ^{195}Pt NMR spectrum of the mixture of $[\mathbf{Pt^{C1}}_2\mathbf{Pt^{C3}}]^{2+}$ with 0.5 eq. of Ag(I) ions exhibited two doublets at −3263 ($^1J_{Pt-Ag}$ = 454 Hz) and −3342 ppm ($^1J_{Pt-Ag}$ = 518 Hz) and one singlet with satellite peaks at −3827 ppm ($^1J_{Pt-Pt}$ = 1743 Hz, $^1J_{Pt-Pt}$ = 1444 Hz) besides a weak broad signal at −3620 ppm (Fig. S15 middle in ESI†). The trinuclear core of $[\mathbf{Pt^{C1}}_2\mathbf{Pt^{C3}}]^{2+}$ contains three inequivalent Pt centres. The two doublet signals showing the coupling with the Ag nucleus are assigned to the Pt centres forming the Ag–Pt bonds in the heptanuclear complex and the

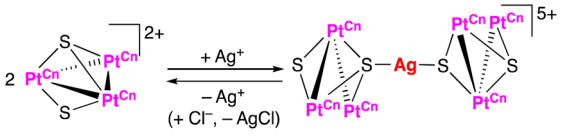

Scheme 3 Reactions of triplatinum complexes with bisNHC-C2 (n = 2), $[\mathbf{Pt^{C2}}_3]^{2+}$, or bisNHC-C3 ligands ($n$ = 3), $[\mathbf{Pt^{C3}}_3]^{2+}$, with 0.5 eq. of Ag(I) ions.

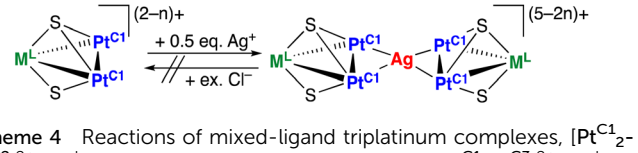

Scheme 4 Reactions of mixed-ligand triplatinum complexes, $[\mathbf{Pt^{C1}}_2\mathbf{Pt^{C2}}]^{2+}$ (M^L = Pt(bisNHC-C2), n = 0) and $[\mathbf{Pt^{C1}}_2\mathbf{Pt^{C3}}]^{2+}$ (M^L = Pt(bisNHC-C3), n = 0), and mixed-metal complex with the {Rh(cod)} moiety, $[\mathbf{Pt^{C1}}_2\mathbf{Rh^{cod}}]^{+}$ (M^L = Rh(cod), n = 1), with 0.5 eq. of Ag(I) ions.

singlet with the satellite peaks is attributed to the Ag-unbound Pt centre. Although the other broad signal should be accompanied with two other signals, they would probably be too weak to be detected due to the low concentration, equilibrium and/or the coupling with Ag and Pt nuclei.

Reactions of mixed-metal diplatinum–rhodium complexes with two {Pt(bisNHC-C1)} and one {Rh(cod)} ($[Pt^{C1}_2Rh^{cod}]^+$) or {RhCp*} ($[Pt^{C1}_2Rh^{Cp*}]^{2+}$) moieties with 0.5 eq. of Ag(I) ions. The mixed-metal trinuclear complex bearing two {Pt(bisNHC-C1)} and one {Rh(cod)} moieties, $[Pt^{C1}_2Rh^{cod}]^+$, exhibits similar behaviours to the mixed-ligand triplatinum complexes, $[Pt^{C1}_2Pt^{C2}]^{2+}$ and $[Pt^{C1}_2Pt^{C3}]^{2+}$, in the reactions with Ag(I) ions (Fig. S9 in ESI†). Thus $[Pt^{C1}_2Rh^{cod}]^+$ reacts with 0.5 eq. of Ag(I) ions to form an M_3AgM_3 heptanuclear complex with the Ag–Pt bonds (Fig. S9(b),† Scheme 4). ^{195}Pt NMR spectrum of the reaction mixture showed one double doublet signal at −3494 ppm ($^1J_{Pt-Ag} = 432$ Hz, $^1J_{Pt-Rh} = 62$ Hz) (Fig. S16 middle in ESI†), whereas $[Pt^{C1}_2Rh^{cod}]^+$ exhibited one singlet signal with no Pt–Rh coupling due to weaker interaction between the Pt and Rh centres. This observation shows the formation of the intermetallic bonds of the Ag centre with the Pt centres and the greater interaction between the Pt and Rh centres appearing in the Pt–Rh coupling. The greater interaction is attributed to the steric repulsion with the bisNHC-C1 ligands caused by the Ag–Pt bond formation, which leads the shrinking of the Pt–Rh bonds. The above results also show that the difference in the charge of the trinuclear complexes is not an important factor for the formation of the heptanuclear complexes.

On the other hand, the Pt_2Rh mixed-metal complex with a {RhCp*} moiety, $[Pt^{C1}_2Rh^{Cp*}]^{2+}$, shows different behaviour in the reaction with Ag(I) ions (Fig. S10 in ESI†). With the addition of 0.5 eq. of Ag(I) ions, at least two species exist in equilibrium (Fig. S10(b)†), whereas the other complexes with the $\{[Pt(bisNHC\text{-}C1)]_2\}$ moiety form the corresponding heptanuclear complexes with Ag–Pt bonds. The ^{195}Pt NMR spectrum for $[Pt^{C1}_2Rh^{Cp*}]^{2+}$ with 0.5 eq. of Ag(I) ions clearly showed a double doublet signal at −3554 ppm ($^1J_{Pt-Ag} = 422$ Hz, $^1J_{Pt-Rh} = 68$ Hz) exhibiting the Ag–Pt bond formation (Fig. S17 middle in ESI†). The observation of the Pt–Rh coupling after the addition of Ag(I) ions also indicates the enhancement of the intermetallic interaction between the Pt and Rh centres while $[Pt^{C1}_2Rh^{Cp*}]^{2+}$ exhibits no Pt–Rh coupling in the ^{195}Pt NMR spectrum (Fig. S17† bottom) due to the weaker intermetallic interaction. Although the ^{1}H NMR spectrum exhibited the signals for more than two species, the ^{195}Pt NMR measurement could not detect the other species probably due to equilibrium of them and the difference of the time scale for ^{1}H and ^{195}Pt NMR spectroscopy. Furthermore, in the case of $[Pt^{C1}_2Rh^{Cp*}]^{2+}$, the extraction of Ag(I) ions by the addition of chloride ions proceeded and reproduced

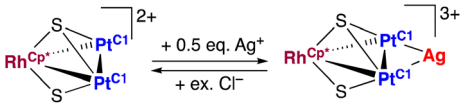

Scheme 5 Reactions of Pt_2Rh complex with a {RhCp*} moiety, $[Pt^{C1}_2Rh^{Cp*}]^{2+}$ with 0.5 eq. of Ag(I) ions.

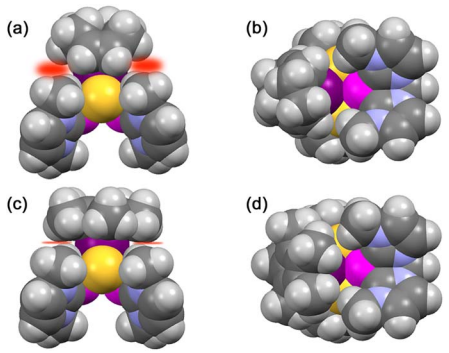

Fig. 8 CPK models of trinuclear complexes bearing {Rh(cod)} ($[Pt^{C1}_2Rh^{cod}]^+$ (a) top view, (b) side view or {RhCp*} ($[Pt^{C1}_2Rh^{Cp*}]^{2+}$ (c) top view, (d) side view. Structures were optimised by DFT calculations.

the ^{1}H NMR signals for the trinuclear complex (Fig. S10(f),† Scheme 5), otherwise the cod complex, $[Pt^{C1}_2Rh^{cod}]^+$, affords the heptanuclear complex in the same condition. This difference is probably ascribed to the steric bulkiness of the incorporated metal–ligand units. The less hindered cod ligand in the trinuclear complex gives more room for the bisNHC-C1 ligands moving to provide the sufficient space in between the methylene bridges for the access of an Ag(I) ion (Fig. 8(a) and (b)). On the other hand, the Cp* complex gives smaller space and the rotation of the Cp* ligand causes further steric repulsion with the methyl substituents (Fig. 8(c) and (d)). As a result, the bisNHC-C1 ligands cannot provide sufficient space to form a stable heptanuclear complex with four Ag–Pt bonds.

Reactions of trinuclear complexes with excess Ag(I) salt

Reactions of triplatinum complexes with bisNHC-C2 ligands ($[Pt^{C2}_3]^{2+}$) with excess Ag(I) ions. The ^{195}Pt NMR spectrum of $[Pt^{C2}_3]^{2+}$ with excess Ag(I) ions exhibited a singlet signal with a larger line width at −3569 ppm (Fig. S12 top in ESI†). Only the C_{3h}-isomer of $[Pt^{C2}_3]^{2+}$ can interact with Ag(I) ions at the sulfide ligands[7] and the addition of Ag(I) ions shifts the equilibrium to the formation of Ag-adducts bearing the Ag–S bonds (Scheme 6). In this point of view, the larger line width of the ^{195}Pt NMR signal for the complex with excess Ag(I) ions suggests the equilibrium among the Ag-adducts with Ag–S bonds (Scheme 6(b)).

Reaction of triplatinum complex with bisNHC-C3 ligands ($[Pt^{C3}_3]^{2+}$) with excess Ag(I) ions. The addition of an excess Ag(I) salt induced more downfield shift of one sharp singlet at −3600 ppm in the ^{195}Pt NMR spectrum (Fig. S13 top in ESI†). This result suggests that the equilibrium among Ag-adducts with the Ag–S bonds shifts to one of them, in which both of the two sulfide ligands coordinate to Ag(I) ions (Scheme 6(b)). Moreover, the ^{195}Pt NMR signal of $[Pt^{C2}_3]^{2+}$ with excess Ag(I) ions is more broaden than that of $[Pt^{C3}_3]^{2+}$ probably due to the more crowded arrangements of the bisNHC-C3 ligands suppressing their flap motion.

From the reaction mixture of $[Pt^{C3}_3]^{2+}$ with excess Ag(I) ions, single crystals were obtained and were analysed by crystallography. Although the quality of the crystals was not suitable for

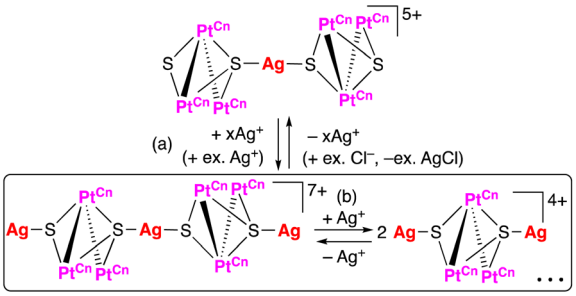

Scheme 6 (a) Coordination of Ag(I) ions to uncoordinated sulfide ligands of heptanuclear complexes with bisNHC-C2 ($n = 2$), $[Pt^{C2}{}_3]^{2+}$, or bisNHC-C3 ligands ($n = 3$), $[Pt^{C3}{}_3]^{2+}$, and (b) dissociation of trinuclear units *via* further coordination of Ag(I) ions to sulfide ligands by the addition of excess Ag(I) ions.

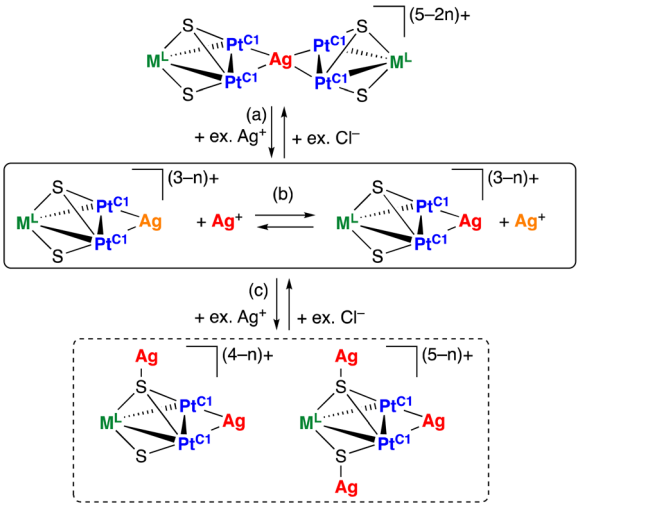

Scheme 7 (a) Dissociation of trimetallic moieties of heptanuclear complexes, (b) exchange reaction of Ag(I) ions for tetranuclear complexes and (c) coordination of Ag(I) ions to sulfide ligands of mixed-ligand triplatinum complexes, $[Pt^{C1}{}_2Pt^{C2}]^{2+}$ (M^L = Pt(bisNHC-C2), $n = 0$) and $[Pt^{C1}{}_2Pt^{C3}]^{2+}$ (M^L = Pt(bisNHC-C3), $n = 0$), and mixed-metal complex with the {Rh(cod)} moiety, $[Pt^{C1}{}_2Rh^{cod}]^{+}$ (M^L = Rh(cod), $n = 1$), with excess Ag(I) ions.

full structural characterisation, the analysis clearly revealed a pentanuclear Ag–Pt_3–Ag framework, in which both sulfide ligands of $[Pt^{C3}{}_3]^{2+}$ coordinate to the Ag(I) ions (Fig. S18 in ESI†). In addition, a nonanuclear Ag-adduct containing two triplatinum moieties with the bisNHC-C2 ligands also crystallised from the reaction mixture with excess Ag(I) ions. In the nonanuclear Ag-adduct, one of the three Ag(I) ions bridges one of the two sulfide ligands of each triplatinum unit and the other sulfide ligands coordinate to the other Ag(I) ions bearing acetonitrile ligands (Fig. 9). Although the bulk preparations of these complexes could not be achieved to collect the data for their characterisation and the results show no proof whether these complexes actually exist in solution, the existence of these Ag-adducts strongly suggests that the species in solution could have the Ag–S bonds and both the sulfide ligands in each triplatinum complex, $[Pt^{C2}{}_3]^{2+}$ or $[Pt^{C3}{}_3]^{2+}$, can coordinate to Ag(I) ions.

Reactions of mixed-ligand triplatinum complexes with two bisNHC-C1 and one bisNHC-C2 ($[Pt^{C1}{}_2Pt^{C2}]^{2+}$) or bisNHC-C3 ($[Pt^{C1}{}_2Pt^{C3}]^{2+}$) with excess Ag(I) ions. Broad ^{1}H NMR signals other than those of the heptanuclear complex appeared in the reaction of $[Pt^{C1}{}_2Pt^{C2}]^{2+}$ with more than 0.5 eq. of Ag(I) ions (Fig. S7(c) and (d) in ESI†) and the intensities of the signals become larger as the amount of Ag(I) ions increased. Only the broad signals were observed for the mixture containing excess Ag(I) ions (Fig. S7(e)†) suggesting the existence of several Ag-adducts in equilibrium (Scheme 7). The ^{195}Pt NMR spectrum of the reaction mixture with excess Ag(I) ions, which showed a broad signal between −3420 and −3390 ppm, supports the formation of the Ag-adducts other than the heptanuclear complex (Fig. S14 top in ESI†). These adducts should involve the additional Ag(I) ions binding to the sulfide ligands. Addition of chloride ions to the reaction mixture containing excess Ag(I) ions (Fig. S7(f)†) restored most of the ^{1}H NMR signals for the heptanuclear complex with Ag–Pt bonds (Fig. S7(b)†), except for those of the 4- and 5-NHC protons appeared in the range of 6.9–7.0 ppm. The chemical shifts of the ^{1}H NMR signals for 4- and 5-NHC protons are often affected by concentration, temperature and/or impurities. Considering this phenomenon, the above results indicate that the sulfide-coordinated Ag(I) ions were removed by the addition of chloride ions from the reaction system as precipitates of AgCl. On the other hand, as expected, the Ag(I) ion bound to the platinum centres in the heptanuclear complex does not react with chloride ions, and the complex maintains its structure in solution.

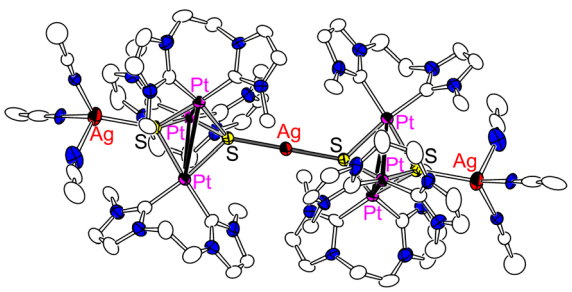

Fig. 9 Structure of nonanuclear Ag-adduct of triplatinum complex bearing three bisNHC-C2 ligands.

The addition of more than 0.5 eq. Ag(I) ions to a solution of $[Pt^{C1}{}_2Pt^{C3}]^{2+}$ afforded broad ^{1}H NMR signals showing some Ag-adducts in equilibrium in solution (Fig. S8(c)–(e) in ESI†) as similar to the case for $[Pt^{C1}{}_2Pt^{C2}]^{2+}$, even though the shapes of the ^{1}H NMR signals for the NHC protons are slightly different. The addition of chloride ions extracts the Ag(I) ions from the adducts leading the regeneration of the heptanuclear complex with Ag–Pt bonds (Fig. S8(f)†). Moreover, in the ^{195}Pt NMR spectrum of the complex with excess Ag(I) ions (Fig. S15 top in ESI†), three singlet signals with satellite peaks appeared at −3359 ($^1J_{Pt–Pt}$ = 1179, $^1J_{Pt–Pt}$ = 478 Hz), −3427 ($^1J_{Pt–Pt}$ = 1165, $^1J_{Pt–Pt}$ = 426 Hz) and −3848 ppm ($^1J_{Pt–Pt}$ = 1205 Hz) besides one weak singlet at −3602 ppm and two small signals at −3943 and −4019 ppm. The signals at −3359 and −3427 ppm appeared in

more downfield if they are compared with those for the trinuclear complex indicating the existence of an Ag-adduct with the Ag–Pt bonds, although no Ag–Pt coupling was observed. The missing of the coupling with Ag nuclei reflects the exchange of the Ag(I) ion in the Ag-adduct (Scheme 7(b)) and suggests the disassembling of the heptanuclear framework affording an Ag-adduct involving one triplatinum unit with two Ag–Pt bonds (Scheme 7(a)). The disassembling of the heptanuclear complex is probably triggered by the coordination of the sulfide ligands to Ag(I) ions and mediated *via* formation of an intermediate bearing Ag–S and Ag–Pt bonds such as a pentanuclear complex described below (Fig. 10). Additionally, Ag-adducts with the Ag–S bonds could exist in the presence of excess Ag(I) ions due to the accessible space around the sulfide ligands (Scheme 7(c)).

Single crystals were obtained from the reaction mixture of $[\mathbf{Pt^{C1}}_2\mathbf{Pt^{C3}}]^{2+}$ with excess Ag(I) ions and analysed by crystallography to reveal a pentanuclear structure that consists of one trinuclear moiety and two Ag(I) ions binding to both of the platinum centres and the sulfide ligands (Fig. 10). The Ag(I) ions are coordinated by bridging and terminal difluorophosphates ($PO_2F_2^-$), which were presumably generated by partial hydrolysis of hexafluorophosphate counter anions during the crystallisation. Some examples for the partial hydrolysis of hexafluorophosphate anion to afford difluorophosphate were reported.[11] Another terminal ligand for the Ag(I) ion was disordered methoxy and acetonitrile ligands with 1 : 1 ratio. The crystallographic result indicates that the cluster cation possesses +1.5 averaged positive charge because the P atom of one of the hexafluorophosphate anion locates at the crystallographic inversion centre. The averaged positive charge of the adduct supports the disordered terminal ligands with equal amounts of the methoxy monoanion and the acetonitrile molecule. The Ag–Ag distance (2.9696(10) Å) is slightly longer than the interatomic distance in metallic silver (2.89 Å) and shorter than the sum of the van der Waals radii of two Ag atoms (3.44 Å)[12] showing the argentophilic interaction.[13] Such interaction for Ag–Ag units bridged by substituted phosphates with an Ag–O–P–O–Ag fashion was reported for Ag–Ag distances of 2.9865(5)–3.1596(3) Å in some Ag clusters.[14] The Ag–Ag unit locates at the least hindered space in between two methylene

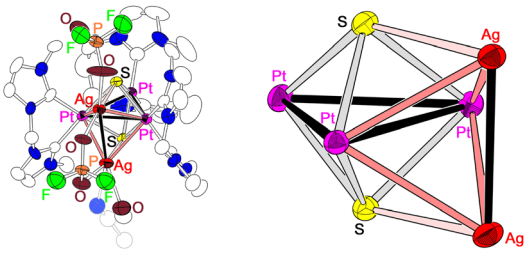

Fig. 10 Structure (left) and framework of metal-sulfide core (right) of pentanuclear Ag-adduct of triplatinum complex bearing two bisNHC-C1 and one bisNHC-C3 ligands. One of the terminal ligands for the Ag(I) ions is disordered CH_3O^- and CH_3CN with 1 : 1 ratio. Selected bond distances (Å): Ag–Ag 2.9696(10); Ag–Pt 2.8895(8), 2.8943(8), 2.8907(8), 2.9003(8); Pt–Pt 3.2786(6), 3.1257(5), 3.1048(5); Ag–S 2.757(3), 2.650(3).

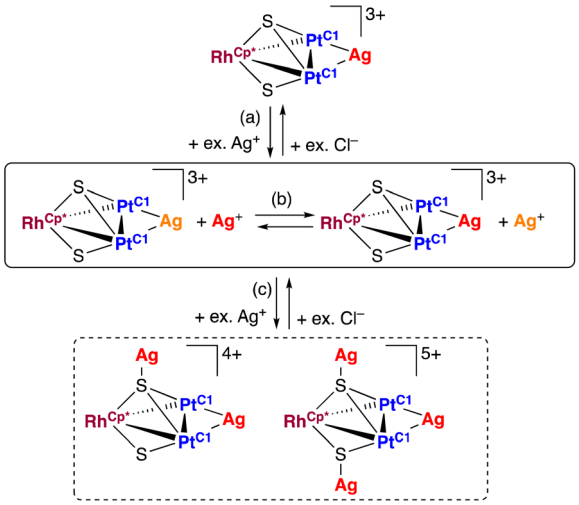

Scheme 8 (a) Addition of excess Ag(I) ions affording (b) exchange reaction of Ag(I) ions and (c) coordination of Ag(I) ions to sulfide ligands of Pt_2Rh complex with a {RhCp*} moiety, $[\mathbf{Pt^{C1}}_2\mathbf{Rh^{Cp^*}}]^{2+}$, with excess Ag(I) ions.

bridges of the bisNHC-C1 ligands similar to the case for the heptanuclear cluster with the bisNHC-C1 triplatinum moieties. The Pt–Pt distance near the Ag(I) ions in the Pt_3Ag_2 pentanuclear complex (3.2786(6) Å) is close to that for the Pt_3AgPt_3 heptanuclear cluster with the bisNHC-C1 ligands (3.2958(5) Å). The Ag–S distances (2.650(3) and 2.757(3) Å) are significantly longer than the typical Ag–S bond lengths (2.34(1)–2.38(1) Å) observed in a silver alkylthiolate complex,[15] for example. However, the Ag–S distances are below the sum of the van der Waals radii of Ag and S atoms (3.52 Å)[12] suggesting a weak interaction between Ag and S atoms. Although the bulk synthesis of the pentanuclear complex could not be achieved, the structure of this adduct clearly indicates that two Ag(I) ions are accessible to the Pt–Pt bond in the {[Pt(bisNHC-C1)]$_2$} dimeric unit of $[\mathbf{Pt^{C1}}_2\mathbf{Pt^{C3}}]^{2+}$.

Summarising the above results of the NMR spectroscopic and crystallographic analyses, the replacement of one of the three bisNHC-C1 ligands in $[\mathbf{Pt^{C1}}_3]^{2+}$ with the bisNHC-C2 or bisNHC-C3 ligand provides the combined steric characters of accessibility to the Pt centres and the sulfide ligands derived from the bisNHC-C1 and bisNHC-C2 or bisNHC-C3 ligands, respectively, for the mixed-ligand triplatinum complexes.

Reactions of mixed-metal diplatinum–rhodium complexes with two {Pt(bisNHC-C1)} and one {Rh(cod)} ($[\mathbf{Pt^{C1}}_2\mathbf{Rh^{cod}}]^+$) or {RhCp*} ($[\mathbf{Pt^{C1}}_2\mathbf{Rh^{Cp^*}}]^{2+}$) moieties with excess Ag(I) ions. The ^{1}H NMR spectra for $[\mathbf{Pt^{C1}}_2\mathbf{Rh^{cod}}]^+$ with more than 0.5 eq. of Ag(I) ions showed one set of additional broad signals for the bisNHC-C1 ligands and the signals for the heptanuclear complex were completely disappeared with excess Ag(I) ions (Fig. S9(c)–(e) in ESI†). The ^{195}Pt NMR measurement showed one broad signal at −3533 ppm (Fig. S16 top in ESI†). The signal appeared in the downfield by hundreds ppm relative to that for the trinuclear complex suggesting the formation of the Ag–Pt bonds. No observation of the Pt–Ag coupling is attributed to the exchange of the Ag(I) ion (Scheme 7(b)). These results mean that the

heptanuclear framework is disassembled to other Ag-adduct bearing one trinuclear unit with two Ag–Pt bonds (Scheme 7(a)). Additionally, the sulfide-coordinated Ag-adducts are possibly involved in equilibrium in solution because of the sufficient space around the sulfide ligands (Scheme 7(c)). Furthermore, the unprotected and/or sulfide-coordinated Ag(I) ions are extracted as AgCl by the addition of chloride ions, resulting in the reformation of the heptanuclear complex (Fig. S9(f) in ESI†).

On the other hand, ^{195}Pt NMR spectrum of $[\mathbf{Pt^{C1}}_2\mathbf{Rh^{Cp^*}}]^{2+}$ in the presence of excess Ag(I) ions showed one doublet signal at −3589 ppm ($^1J_{\mathrm{Pt-Rh}} = 120$ Hz) besides two weak signals at −3676 and 3603 ppm (Fig. S17 top in ESI†). Because the Pt–Ag coupling is missing due to the exchange of the Ag(I) ion and the formation of the Ag–Pt bonds leads downfield shift of ^{195}Pt NMR signals by hundreds ppm, the doublet signal is assignable to the Ag-bound Pt centres (Scheme 8(b)). These results imply the formation of a $AgPt_2Rh$ tetranuclear complex. The two weak signals are probably attributed to the unsymmetric isomer of the tetranuclear complex bearing the trinuclear unit with the (Me^{C1}-Alk^{C1})-isomeric form, which involves two inequivalent Pt centres. Additionally, in the presence of excess Ag(I) ions, the Ag-adducts with the Ag–S bonds possibly form because of the accessible spaces around the sulfide ligands (Scheme 8(c)).

Conclusions

In this study, we demonstrated that NHC ligands with strong σ-donation ability enhance the reactivity of trinuclear complexes bearing bisNHC-platinum units with Ag(I) ions. We also evaluated the steric effects of bisNHC ligands with a variety of alkylene bridges, which affect the dihedral angles between each of two NHC planes and the coordination plane, using reactions of Ag(I) ions with trinuclear complexes exhibiting striking steric repulsions. The bisNHC-C1 ligands in the trinuclear complexes make large steric bulkiness around the sulfide ligands but provide sufficient space for an Ag(I) ion to form Ag–Pt bonds. On the other hand, bisNHC-C2 and bisNHC-C3 ligands, which have more-folded structures, provide sufficient space for Ag(I) ions approaching to the sulfide ligands but prevent the Ag–Pt bond formation. In the mixed-ligand system, the complexes have the characters of both bisNHC-C1 and the other bis-NHC complexes. For the mixed-metal complexes with the {[Pt(bisNHC-C1)]$_2$} unit, the larger Cp* ligand in the complex prevents the formation of the corresponding heptanuclear complex, whereas the complex with the relatively smaller cod ligand exhibits similar reactivity to the mixed-ligand complexes to form the heptanuclear complex.

The steric bulkiness of the bis-NHC ligands around the Pt–Pt bond and the sulfide ligands corresponds to that around the unoccupied virtual axial positions and the coordination sites of the square planar Pt(II) centre, respectively. In this point of view, the bisNHC-C1 ligand causes more steric repulsion than the bisNHC-C2 and bisNHC-C3 ligands around the coordination sites of square planar complexes such as palladium complexes, which are used for catalysts of coupling reactions. On the other hand, bisNHC-C2 and bisNHC-C3 ligands greatly affect the steric bulkiness around the unoccupied virtual axial positions of square planar complexes. The results obtained in this study will provide useful information for designing novel NHC complex catalysts for selective reactions.

Experimental section

General procedures

All chemicals were purchased from Sigma-Aldrich, Nacalai Tesque and Wako Pure Chemical Industries. All reagents and solvents were used as received. *cis*-[Pt(bisNHC-C1)Cl_2], *cis*-[Pt(bisNHC-C1)$(NCCH_3)_2$](OTf)$_2$, *cis*-[Pt(bisNHC-C3)$(NCCH_3)_2$]$(PF_6)_2$ and *cis*-[Pt(bisNHC-C*n*)$(SH)_2$] (bisNHC-C*n* = 1,1′-dimethyl-3,3′-X-4-diimidazolilydene ($n = 1$, X = methylene; $n = 2$, X = ethylene; $n = 3$, propylene)), were prepared according to the reported procedures.[16] [(RhCp*Cl)$_2$(μ-Cl)$_2$] was synthesised using a previously reported procedure.[17] ^{1}H, ^{13}C and ^{195}Pt NMR spectra were recorded on Bruker AVANCE 400 or 600 FT-NMR spectrometers. Chemical shifts (δ in ppm, coupling constants J in Hz) for ^{1}H and ^{13}C NMR signals are expressed from $SiMe_4$ and referenced to residual solvent resonances (Fig. S19–S28 in ESI†). Chemical shifts for ^{195}Pt signals were externally referenced to the signal of 1.2 mol L^{-1} $Na_2[PtCl_6]$ in D_2O (Fig. S11–S17 in ESI†). Elemental analyses were performed on a J-Science Lab JM-10 elemental analyser by the Analytical Research Centre at Osaka Metropolitan University. Electrospray ionisation mass spectrometry was performed on JEOL AccuTOF LC-plus JMS-T100LP spectrometer.

Synthesis of [{Pt(bisNHC-C3)}$_3$(μ$_3$-S)$_2$](PF$_6$)$_2$ ([Pt^{C3}$_3$](PF$_6$)$_2$)

A solution of *cis*-[Pt(bisNHC-C3)}$(SH)_2$] (0.10 g, 0.22 mmol) and *cis*-[{Pt(bisNHC-C3)}$(NCCH_3)_2$]$(PF_6)_2$ (0.35 g, 0.45 mmol) in DMSO (35 mL) was stirred for 25 min and heated at 60 °C for 2 h to give a yellow solution. $KHCO_3$ (0.58 g, 5.8 mmol) was added to the solution and the mixture was stirred for 20 min. The solvent was removed under reduced pressure to give a white-yellow solid. The solid was re-dissolved in water (10 mL). To the resulted solution was added a solution of NH_4PF_6 (0.84 g 5.1 mmol) in water (5 mL) to give a white-yellow solid. The solid was collected by suction filtration, washed with water (14 mL) and air-dried. Yield: 0.32 g, 96%. Single crystals suitable for X-ray crystallography were obtained by slow evaporation of the solvents from a solution in a mixture of acetonitrile and toluene. Anal. calcd for [{Pt(bisNHC-C3)}$_3$(μ$_3$-S)$_2$](PF$_6$)$_2$ (C_{33}-$H_{48}F_{12}N_{12}P_2Pt_3S_2$): C, 25.54; H, 3.12; N, 10.83, found: C, 26.03 H, 3.59; N, 10.72. MS (ESI+, CH_3CN): m/z = 631 ([Pt^{C3}$_3$]$^{2+}$), 1406 ([[Pt^{C3}$_3$](PF$_6$)]$^+$).

Synthesis of [{Pt(bisNHC-C1)}$_2$Pt(bisNHC-C2)}(μ$_3$-S)$_2$](PF$_6$)$_2$ ([Pt^{C1}$_2$Pt^{C2}](PF$_6$)$_2$)

A mixture of *cis*-[Pt(bisNHC-C2)$(SH)_2$] (0.023 g, 0.05 mmol), *cis*-[Pt(bisNHC-C1)Cl_2] (0.046 g, 0.10 mmol) and $KHCO_3$ (0.26 g, 2.6 mmol) in DMSO (19 mL) was stirred for 10 min to give a yellow mixture, which was heated at 60 °C for 4 h to afford a pale-yellow mixture. The solvent was removed under reduced pressure to give a pale-yellow solid. The solid was re-dissolved in water (5

mL) and added a solution of NH_4PF_6 (0.21 g 1.3 mmol) in water (10 mL) to give a white solid, which was collected by suction filtration, washed with water (15 mL) and air-dried. Yield: 0.057 g, 74%. The sample for elemental analysis was purified by the addition of diethyl ether to a solution of the complex in acetonitrile. Single crystals suitable for X-ray crystallography were obtained from a solution in a mixture of acetonitrile and toluene by slow evaporation of the solvents. Anal. calcd for $[\{Pt(bisNHC\text{-}C1)\}_2\{Pt(bisNHC\text{-}C2)\}(\mu_3\text{-}S)_2](PF_6)_2\cdot 0.5Et_2O$ ($C_{30}H_{43}F_{12}N_{12}O_{0.5}P_2Pt_3S_2$): C, 23.72; H, 2.85; N, 11.07, found: C, 23.76; H, 2.83; N, 11.02. MS (ESI+, CH_3CN): m/z = 596 ($[\mathbf{Pt^{C1}}_2\mathbf{Pt^{C2}}]^{2+}$), 1336 ($[[\mathbf{Pt^{C1}}_2\mathbf{Pt^{C2}}](PF_6)]^+$).

Synthesis of $[\{Pt(bisNHC\text{-}C1)\}_2\{Pt(bisNHC\text{-}C3)\}(\mu_3\text{-}S)_2](PF_6)_2$ ($[\mathbf{Pt^{C1}}_2\mathbf{Pt^{C3}}](PF_6)_2$)

A mixture of *cis*-$[Pt(bisNHC\text{-}C3)(SH)_2]$ (0.024 g, 0.05 mmol), *cis*-$[Pt(bisNHC\text{-}C1)Cl_2]$ (0.046 g, 0.10 mmol) and $KHCO_3$ (0.11 g, 1.1 mmol) in DMSO (19 mL) was stirred for 10 min to give a yellow mixture, which was heated at 60 °C for 4 h to afford a pale-yellow mixture. The solvent was removed under reduced pressure to give a pale-yellow solid. The solid was re-dissolved in water (5 mL) and added a solution of NH_4PF_6 (0.071 g 0.43 mmol) in water (10 mL) to give a white solid, which was collected by suction filtration, washed with water (15 mL) and air-dried. Yield: 0.040 g, 53%. Single crystals suitable for X-ray crystallography were obtained by slow evaporation of the solvents from a solution in a mixture of acetonitrile, methanol and toluene. Anal. calcd for $[\{Pt(bisNHC\text{-}C1)\}_2\{Pt(bisNHC\text{-}C3)\}(\mu_3\text{-}S)_2](PF_6)_2\cdot 2H_2O$ ($C_{29}H_{44}F_{12}N_{12}O_2P_2Pt_3S_2$): C, 22.74; H, 2.89; N, 10.97, found: C, 22.82; H, 2.82; N, 11.05. MS (ESI+, CH_3CN): m/z = 603 ($[\mathbf{Pt^{C1}}_2\mathbf{Pt^{C3}}]^{2+}$), 1350 ($[[\mathbf{Pt^{C1}}_2\mathbf{Pt^{C3}}](PF_6)]^+$).

Synthesis of $[\{Pt(bisNHC\text{-}C1)\}_2\{Rh(cod)\}(\mu_3\text{-}S)_2](PF_6)$ ($[\mathbf{Pt^{C1}}_2\mathbf{Rh^{cod}}](PF_6)$)

A solution of *cis*-$[Pt(bisNHC\text{-}C1)Cl_2]$ (0.023 g, 0.05 mmol) in DMSO (2 mL) was added to a solution of *cis*-$[Pt(bisNHC\text{-}C1)(SH)_2]$ (0.021 g, 0.05 mmol) in DMSO (5 mL) to give a yellow solution. The solution was stirred for 10 min. A solution of $[\{Rh(cod)\}_2\{\mu\text{-}Cl\}_2]$ (0.013 g, 0.026 mmol) in DMSO (2 mL) was added to the yellow solution, and then $KHCO_3$ (0.15 g, 1.5 mmol) was added to the solution to give a blown mixture. After the mixture was stirred for 30 min, the solvent was removed under reduced pressure to give a yellow solid. The solid was re-dissolved in water (5 mL) and added a solution of NH_4PF_6 (0.11 g, 0.69 mmol) in water (5 mL) to give a dark-brown solid, which was collected by suction filtration, washed with water (6 mL) and air-dried. Yield: 0.047 g, 84%. Single crystals suitable for X-ray crystallography were obtained by slow diffusion of diethyl ether into a solution in acetonitrile. Anal. calcd for $[\{Pt(bisNHC\text{-}C1)\}_2\{Rh(cod)\}(\mu_3\text{-}S)_2](PF_6)\cdot 0.75(Et_2O)\cdot H_2O$ ($C_{29}H_{45.5}F_6N_8O_{1.75}P\ Pt_2RhS_2$): C, 28.17; H, 3.71; N, 9.06. Found: C, 28.32; H, 3.81; N, 9.29. MS (ESI+, CH_3CN): m/z = 1017 ($[\mathbf{Pt^{C1}}_2\mathbf{Rh^{cod}}]^+$).

Synthesis of $[\{Pt(bisNHC\text{-}C1)\}_2(RhCp^*)(\mu_3\text{-}S)_2](PF_6)_2$ ($[\mathbf{Pt^{C1}}_2\mathbf{Rh^{Cp^*}}](PF_6)_2$)

A solution of AgOTf (0.026 g, 0.10 mmol) in CH_3CN (5 mL) was added to a solution of $[(RhCp^*Cl)_2(\mu\text{-}Cl)_2]$ (0.016 g, 0.026 mmol) and the mixture was stirred for 2 h to give an AgCl solid. The solid was removed by centrifugation to afford an orange solution. Diethyl ether was added to the solution to give red and grey precipitates. The solid was re-dissolved in CH_3CN (5 mL) and the insoluble solid was removed using a membrane filter. The obtained orange filtrate and $KHCO_3$ (0.027 g, 0.27 mmol) were added to a reaction mixture, which was obtained by the reaction of *cis*-$[Pt(bisNHC\text{-}C1)(SH)_2]$ (0.023 g, 0.053 mmol) and *cis*-$[Pt(bisNHC\text{-}C1)(NCCH_3)_2](OTf)_2$ (0.037 g, 0.049 mmol) in DMSO (10 mL) with stirring for 10 min. After the mixture was stirred for 2 h, the solvent was removed under reduced pressure to give a dark-green solid. Water (15 mL) was added to the solid and an insoluble solid was collected by suction filtration, washed with diethylether and air-dried. Yield: 0.034 g, 57%.

A solution of $NaBPh_4$ (0.36 g, 1.0 mmol) in CH_3OH (2 mL) was added to a solution of $[\mathbf{Pt^{C1}}_2\mathbf{Rh^{Cp^*}}](OTf)_2$ (0.067 g, 0.05 mmol) in methanol (2 mL) to give $[\mathbf{Pt^{C1}}_2\mathbf{Rh^{Cp^*}}](BPh_4)_2$ as a white-green solid. The solid was collected by suction filtration. Yield: 0.072 g, 85%.

A solution of PPh_4Cl (0.031 g, 0.083 mmol) in dichloromethane (2 mL) was added to a mixture of the $[\mathbf{Pt^{C1}}_2\mathbf{Rh^{Cp^*}}](BPh_4)_2$ (0.072 g, 0.043 mmol) in dichloromethane (10 mL) and acetonitrile (2 mL) and the mixture was stirred for 30 min. The solvent was removed under reduced pressure to give a white-green solid. The solid was dissolved in water (10 mL) and an insoluble white-solid was removed by suction filtration. The solvent was removed under reduced pressure to give $[\mathbf{Pt^{C1}}_2\mathbf{Rh^{Cp^*}}]Cl_2$ as a green filmed solid. The solid was collected by suction filtration using acetone and diethyl ether. Yield: 0.021 g, 44%.

A solution of NH_4PF_6 (0.033 g, 0.20 mmol) in water (5 mL) was added to a solution of $[\mathbf{Pt^{C1}}_2\mathbf{Rh^{Cp^*}}]Cl_2$ (0.021 g, 0.019 mmol) in water (5 mL) to give $[\mathbf{Pt^{C1}}_2\mathbf{Rh^{Cp^*}}](PF_6)_2$ as a green solid. The solid was collected by suction filtration and washed with water. Yield: 0.0065 g, 23%.

Single crystals of the BPh_4 salt suitable for X-ray crystallography were obtained by slow diffusion of cyclohexane into a solution of the BPh_4 salt in a mixture of acetonitrile, dichloromethane and a small amount of water. Anal. calcd for $[\{Pt(bisNHC\text{-}C1)\}_2(RhCp^*)(\mu_3\text{-}S)_2](PF_6)_2\cdot CH_3CN\cdot H_2O$ ($C_{30}H_{44}F_{12}\ N_9OP_2Pt_2RhS_2$): C, 25.85; H, 3.18; N, 9.04. Found: C, 25.65; H, 3.24; N, 8.75. MS (ESI+, CH_3CN): m/z = 522 ($[\mathbf{Pt^{C1}}_2\mathbf{Rh^{Cp^*}}]^{2+}$), 1189 ($[[\mathbf{Pt^{C1}}_2\mathbf{Rh^{Cp^*}}](PF_6)]^+$).

Reaction of trinuclear complexes with Ag(I) ions

For the investigation of the reactions of the trinuclear complexes and Ag^+, samples for ^1H NMR measurements were prepared using solutions of trinuclear complexes in CD_3CN (10 mmol L^{-1}, 2 mL) with 0.5, 1, 5 or 20 eq. of $AgPF_6$. For the extraction of Ag(I) ions from the reaction system, 40 eq. of NH_4Cl was added to the solutions with excess Ag^+.

Single crystals of the Ag-adducts with triplatinum complexes with three bisNHC-C2 or bisNHC-C3 ligands were obtained from respective solutions of the complexes in acetonitrile with excess amount of $AgPF_6$ by diffusion of diethyl ether after the addition of a small amount of methanol.

In the case of the Ag-adduct containing a triplatinum moiety with two bisNHC-C1 and bisNHC-C3 ligands and two Ag(I) ions coordinated by difluorophosphate ligands, single crystals for the X-ray crystallographic measurement were obtained as follows. To a solution of the mixed-ligand triplatinum complex (9.7 mmol L^{-1}, 1 mL) with (9.2 mg, 3.8 μmol), methanol (*ca.* 0.5 mL) was added followed by the addition of a small amount of toluene to afford a tiny amount of white solids. After the solids were removed using a membrane filter, the filtrate was allowed to evaporate the solvents resulting in crystallisation of the Ag-adduct.

X-ray crystallography

Single crystals of $[\mathbf{Pt^{C2}_3}](PF_6)_2$, $[\mathbf{Pt^{C3}_3}](PF_6)_2$, $[\mathbf{Pt^{C1}_2Pt^{C2}}](PF_6)_2$, $[\mathbf{Pt^{C1}_2Pt^{C3}}](PF_6)_2$, $[\mathbf{Pt^{C1}_2Rh^{cod}}](PF_6)$, $[\mathbf{Pt^{C1}_2Rh^{Cp^*}}](BPh_4)_2$ and Ag-adducts of $[\mathbf{Pt^{C2}_3}]^{2+}$, $[\mathbf{Pt^{C1}_2Pt^{C3}}]^{2+}$ and $[\mathbf{Pt^{C3}_3}]^{2+}$ were mounted on a loop using Paratone. Diffraction data were collected on a Rigaku Varimax Saturn724 diffractometer using a rotation method with 0.5° frame widths. The data were integrated, scaled, sorted, and averaged using the CrystalClear[18] software. Absorption corrections were applied using the multi-scan method. The structures were solved using SHELXS97 (ref. 19) and refined with SHELXL Version 2018/3 (ref. 20) using the CrystalStructure software[21] or version of olex2.refine 1.5-dev.[22] All hydrogen atoms were located at the calculated positions and refined as riding models. Crystallographic data are summarised in Tables S1–S9 in ESI.†

DFT calculations

DFT calculations were carried out on the isomers of trinuclear complex cations, which were observed in crystallographic analyses for $[\mathbf{Pt^{C1}_2Rh^{cod}}]^+$ and $[\mathbf{Pt^{C1}_2Rh^{Cp^*}}]^{2+}$ using Gaussian 09.[23] Atomic coordinates were optimised at the level of B3LYP/LanL2DZ. Structural optimisations were started from the structures obtained from crystallographic analyses. Vibrational frequencies were calculated for all converged structures, and no imaginary frequencies appeared showing that these structures lie on minima. The atomic coordinates of the optimised structures of the complexes are listed in Tables S10 and S11 in ESI.†

Data availability

The data supporting this article have been included as part of the ESI.† Crystallographic data for $[\mathbf{Pt^{C2}_3}](PF_6)_2$, $[\mathbf{Pt^{C3}_3}](PF_6)_2$, $[\mathbf{Pt^{C1}_2Pt^{C2}}](PF_6)_2$, $[\mathbf{Pt^{C1}_2Pt^{C3}}](PF_6)_2$, $[\mathbf{Pt^{C1}_2Rh^{Cp^*}}](BPh_4)_2$, $[\mathbf{Pt^{C1}_2Rh^{cod}}](PF_6)$, $[Ag\{[Pt(bisNHC\text{-}C2)]_3[Ag(NCCH_3)_3](m_4\text{-}S)_2\}_2](PF_6)_7$ and $[\{Pt(bisNHC\text{-}C1)\}_2\{Pt(bisNHC\text{-}C3)\}(m_4\text{-}S)_2\{Ag(O_2PF_2)\}\{Ag(NCCH_3)_{0.5}(OCH_3)_{0.5}\}(m\text{-}O_2PF_2)](PF_6)_{1.5}$ has been deposited at the CCDC under 2238719–2238726 and can be obtained from **https://www.ccdc.cam.ac.uk**.

Author contributions

Natsuki Yabune: conceptualisation, funding acquisition, investigation, visualisation and writing – original draft. Hiroshi Nakajima: writing – review & editing. Takanori Nishioka: funding acquisition, project administration, supervision, visualisation and writing – original draft.

Conflicts of interest

There are no conflicts to declare.

Acknowledgements

This work was supported by JSPS KAKENHI Grant Numbers N22K05146 and K22KJ2607.

Notes and references

1 C. A. Tolman, *Chem. Rev.*, 1977, **77**, 313–348.
2 (*a*) A. Poster, B. Cosenza, A. Correa, S. Giudice, F. Ragone, V. Scarano and L. Cavallo, *Eur. J. Inorg. Chem.*, 2009, 1759–1766; (*b*) L. Falivene, Z. Cao, A. Petta, L. Serra, A. Poater, R. Olive, V. Scarano and L. Cavallo, *Nat. Chem.*, 2019, **11**, 872–879; (*c*) A. Collado, J. Balogh, S. Meiries, A. M. Z. Slawin, L. Falivene, L. Cavallo and S. P. Nolan, *Organometallics*, 2013, **32**, 3249–3252; (*d*) M. S. Viciu, O. Navarro, R. F. Germaneau, R. A. Kelly III, W. Sommer, N. Marion, E. D. Stevens, L. Cavallo and S. P. Nolan, *Organometallics*, 2004, **23**, 1629–1635; (*e*) S. Gaillard, X. Bantreil, A. M. Z. Slawin and S. P. Nolan, *Dalton Trans.*, 2009, 6967–6971; (*f*) H. Clavier, A. Correa, L. Cavallo, E. C. Escudero-Adán, J. Benet-Buchholz, A. M. Z. Slawin and S. P. Nolan, *Eur. J. Inorg. Chem.*, 2009, **13**, 1767–1773; (*g*) C. A. Urbina-Blanco, X. Bantreil, H. Clavier, A. M. Z. Slawin and S. P. Nolan, *Beilstein J. Org. Chem.*, 2010, **6**, 1120–1126; (*h*) X. Bantreil, R. A. M. Randall, A. M. Z. Slawin and S. P. Nolan, *Organometallics*, 2010, **29**, 3007–3011; (*i*) H. Clavier and S. P. Nolan, *Chem. Commun.*, 2010, **46**, 841–861; (*j*) S. Gaillard, A. M. Z. Slawin, A. T. Bonura, E. D. Stevens and S. P. Nolan, *Organometallics*, 2010, **29**, 394–402; (*k*) S. R. Patrick, A. Collado, S. Meiries, A. M. Z. Slawin and S. P. Nolan, *J. Organomet. Chem.*, 2015, **775**, 152–154; (*l*) A. Gómez-Suárez, D. J. Nelson and S. P. Nolan, *Chem. Commun.*, 2017, **53**, 2650–2660; (*m*) D. Gasperini, M. D. Greenhalgh, R. Imad, S. Siddiqui, A. Malik, F. Arshad, M. I. Choudhary, A. M. Al-Majid, D. B. Cordes, A. M. Z. Slawin, S. P. Nolan and A. D. Smith, *Chem.–Eur. J.*, 2019, **25**, 1064–1075.
3 S. Byun, H. Seo, J.-H. Choi, J. Y. Ryu, J. Lee, W.-J. Chung and S. Hong, *Organometallics*, 2019, **38**, 4121–4132.
4 (*a*) S. K. U. Riederer, P. Gigler, M. P. Högerl, E. Herdtweck, B. Bechlars, W. A. Herrmann and F. E. Kühn, *Organometallics*, 2010, **29**, 5681–5692; (*b*) S. Ahrens, A. Zeller, M. Taige and T. Strassner, *Organometallics*, 2006, **25**, 5409–5415; (*c*) J. A. Mata, M. Poyatos and E. Peris, *Coord. Chem. Rev.*, 2007, **251**, 841–859; (*d*) M. G. Gardiner

and C. C. Ho, *Coord. Chem. Rev.*, 2018, **375**, 373–388; (*e*) Y. Maeda, H. Hashimoto, I. Kinoshita and T. Nishioka, *Inorg. Chem.*, 2014, **53**, 661–663.

5 Y. Maeda, H. Hashimoto and T. Nishioka, *Dalton Trans.*, 2012, **41**, 12038–12047.

6 N. Yabune, H. Nakajima and T. Nishioka, *Dalton Trans.*, 2020, **49**, 7680–7683.

7 N. Yabune, H. Nakajima and T. Nishioka, *Dalton Trans.*, 2021, **50**, 12079–12082.

8 (*a*) J. Ruiz, V. Rodríguez, A. Pérez, G. López and D. Bautista, *J. Organomet. Chem.*, 2004, **689**, 2080–2086; (*b*) S.-W. A. Fong, T. S. A. Hor, S. M. Devoy, B. A. Waugh, B. K. Nicholson and W. Henderson, *Inorg. Chim. Acta*, 2004, **357**, 2081–2090; (*c*) B. C. White, D. Harrison, W. Henderson, B. K. Nicholson and T. S. A. Hor, *Inorg. Chim. Acta*, 2010, **363**, 2387–2393; (*d*) R. B. Sutton and W. Henderson, *Inorg. Chim. Acta*, 2020, **506**, 119557; (*e*) Z. Li, H. Liu, K. F. Mok, A. S. Batsanov, J. A. K. Howard and T. S. A. Hor, *J. Organomet. Chem.*, 1999, **575**, 223–231; (*f*) R. Mas-Ballesté, P. A. Champkin, W. Clegg, P. González-Duarte, A. Lledós and G. Ujaque, *Organometallics*, 2004, **23**, 2522–2532; (*g*) S. Jeram, W. Henderson, B. K. Nicholson and T. S. A. Hor, *J. Organomet. Chem.*, 2006, **691**, 2827–2838.

9 Y. Maeda, H. Hashimoto, I. Kinoshita and T. Nishioka, *Inorg. Chem.*, 2015, **54**, 448–459.

10 O. Hiltner, F. J. Boch, L. Brewitz, P. Härter, M. Drees, E. Herdtweck, W. A. Herrmann and F. E. Kühn, *Eur. J. Inorg. Chem.*, 2010, 5284–5293.

11 (*a*) M. Ferrer, A. Gallen, A. Gutiérrez, M. Martínez, E. Ruiz, Y. Lorenz and M. Engeser, *Chem.–Eur. J.*, 2020, **26**, 7847–7860; (*b*) F. Santoro, M. Althaus, C. Bonaccorsi, S. Gischig and A. Mezzetti, *Organometallics*, 2008, **27**, 3866–3878; (*c*) A. K. Jain, M. R. Gau, P. J. Carroll and K. I. Goldberg, *Organometallics*, 2022, **41**, 3341–3348; (*d*) A. B. McQuarters, J. W. Kampf, E. E. Alp, M. Hu, J. Zhao and N. Lehnert, *Inorg. Chem.*, 2017, **56**, 10513–10528; (*e*) D. L. Gerlach, S. Siek, D. B. Burks, J. M. Tesh, C. R. Thompson, R. M. Vasquez, N. J. White, M. Zeller, D. B. Grotjahn and E. T. Papish, *Inorg. Chim. Acta*, 2017, **466**, 442–450; (*f*) I. T. Chizhevsky, N. V. Rastova, N. E. Kolobova, P. V. Petrovskii, E. I. Fedin, L. E. Vinogradova, L. A. Leites, A. I. Yanovsky and Yu. T. Struchkov, *J. Organomet. Chem.*, 1988, **339**, 165–180.

12 A. Bondi, *J. Phys. Chem.*, 1965, **68**, 441–451.

13 (*a*) M. Jansen, *Angew. Chem., Int. Ed.*, 1987, **26**, 1098–1110; (*b*) P. Majumdar, K. K. Kamar, S. Goswami and A. Castineiras, *Chem. Commun.*, 2001, 1292–1293; (*c*) X.-D. Chen, M. Du and T. C. W. Mak, *Chem. Commun.*, 2005, 4417–4419.

14 (*a*) J. A. Fry, C. R. Samanamu, J.-L. Montchamp and A. F. Richards, *Eur. J. Inorg. Chem.*, 2008, 463–470; (*b*) C. R. Samanamu, E. N. Zamora, J.-L. Montchamp and A. F. Richards, *J. Solid State Chem.*, 2008, **181**, 1462–1471; (*c*) V. Moodley, L. Mthethwa, M. N. Pillay, B. Omondi and W. E. van Zyl, *Polyhedron*, 2015, **99**, 87–95.

15 I. G. Dance, L. J. Fitzpatrick, A. D. Rae and M. L. Scudder, *Inorg. Chem.*, 1983, **22**, 3785–3788.

16 (*a*) M. Muehlhofer, T. Strassner, E. Herdtweck and W. A. Herrmann, *J. Organomet. Chem.*, 2002, **660**, 121–126; (*b*) Y. Unger, A. Zeller, M. A. Taige and T. Strassner, *Dalton Trans.*, 2009, 4786–4794.

17 C. White, A. Yates, P. M. Maitlis and D. M. Heinekey, *Inorg. Synth.*, 1992, **29**, 228–234.

18 CrystalClear, Rigaku Corporation, *CrystalClear Software User's Guide, Molecular Structure Corporation*, 1999; J. W. Pflugrath, *Acta Crystallogr., Sect. D: Biol. Crystallogr.*, 1999, **55**, 1718–1725.

19 SHELXL97 and G. M. Sheldrick, *Program for Crystal Structure Refinement*, University of Göttingen, Göttingen, Germany, 1997.

20 G. M. Sheldrick, *Acta Crystallogr., Sect. A: Found. Crystallogr.*, 2008, **64**, 112–122.

21 CrystalStructure 4.3, *Crystal Structure Analysis Package*, Rigaku Corporation, 2000–2019, Tokyo 196-8666, Japan.

22 (*a*) L. J. Bourhis, O. V. Dolomanov, R. J. Gildea, J. A. K. Howard and H. Puschmann, The Anatomy of a Comprehensive Constrained, Restrained, Refinement Program for the Modern Computing Environment – Olex2 Dissected, *Acta Crystallogr., Sect. A: Found. Adv.*, 2015, **71**, 59–71; (*b*) O. V. Dolomanov, L. J. Bourhis, R. J. Gildea, J. A. K. Howard and H. Puschmann, Olex2: a complete structure solution, refinement and analysis program, *J. Appl. Crystallogr.*, 2009, **42**, 339–341.

23 Gaussian 09, Revision A.02, M. J. Frisch, G. W. Trucks, H. B. Schlegel, G. E. Scuseria, M. A. Robb, J. R. Cheeseman, G. Scalmani, V. Barone, G. A. Petersson, H. Nakatsuji, X. Li, M. Caricato, A. Marenich, J. Bloino, B. G. Janesko, R. Gomperts, B. Mennucci, H. P. Hratchian, J. V. Ortiz, A. F. Izmaylov, J. L. Sonnenberg, D. Williams-Young, F. Ding, F. Lipparini, F. Egidi, J. Goings, B. Peng, A. Petrone, T. Henderson, D. Ranasinghe, V. G. Zakrzewski, J. Gao, N. Rega, G. Zheng, W. Liang, M. Hada, M. Ehara, K. Toyota, R. Fukuda, J. Hasegawa, M. Ishida, T. Nakajima, Y. Honda, O. Kitao, H. Nakai, T. Vreven, K. Throssell, J. A. Montgomery Jr, J. E. Peralta, F. Ogliaro, M. Bearpark, J. J. Heyd, E. Brothers, K. N. Kudin, V. N. Staroverov, T. Keith, R. Kobayashi, J. Normand, K. Raghavachari, A. Rendell, J. C. Burant, S. S. Iyengar, J. Tomasi, M. Cossi, J. M. Millam, M. Klene, C. Adamo, R. Cammi, J. W. Ochterski, R. L. Martin, K. Morokuma, O. Farkas, J. B. Foresman and D. J. Fox, *Gaussian, Inc.*, Wallingford CT, 2016.